RSC Advances

PAPER

View Article Online
View Journal | View Issue

Cite this: *RSC Adv.*, 2017, **7**, 47738

Study on the anti-abrasion resistance of superhydrophobic coatings based on fluorine-containing acrylates with different T_g and SiO_2†

Kunquan Li,[ab] Xingrong Zeng,*[a] Xuejun Lai[a] and Shengyong Chai[b]

Fluorine-containing acrylates (FACs) with different glass transition temperature (T_g) were synthesized by solution copolymerization, and then the superhydrophobic coatings were fabricated based on the FAC, micro-SiO_2 (M-SiO_2) and nano-SiO_2 (N-SiO_2) particles through a two-step spray method. The prepared FAC was characterized by Fourier transform infrared spectroscopy (FTIR), proton nuclear magnetic resonance (^{1}H-NMR) and differential scanning calorimetry (DSC). The wetting behavior and surface morphology of the superhydrophobic coating were studied. The resistance and mechanism of the superhydrophobic coating against abrasion were also investigated. FTIR and ^{1}H-NMR showed that the fluorinated-containing monomer had copolymerized with the acrylate monomers, and FACs with different T_g of about 74.2 °C, 24.5 °C, −7.7 °C and −29.5 °C were prepared. After coating with FAC/M-SiO_2/N-SiO_2 composite coating, the surface showed hierarchical structures with a roughness (S_a) of 1.23 mm, and became superhydrophobic with a water contact angle higher than 150° and a low sliding angle lower than 5°. Abrasion testing showed that the superhydrophobic coating fabricated based on the FAC polymer with low T_g had better abrasion resistance in comparison with that of the FAC polymer with high T_g. Meanwhile, the M-SiO_2 in the composite coating could weaken the abrasion force to the surface micro roughness damage and acted as connections for the adhesion of N-SiO_2 particles during abrasion, which ensured the binary micro/nano structures required for good hydrophobicity after abrasion.

Received 17th July 2017
Accepted 4th October 2017

DOI: 10.1039/c7ra07865j

rsc.li/rsc-advances

1. Introduction

Recently, the superhydrophobic surface, inspired from the lotus leaf, has gained great interest because of its special water repellent property.[1,2] A water droplet remains spherical on the superhydrophobic surface with a high water contact angle above 150°, and can easily roll down and takes the dirt away when the surface inclines at a low sliding angle (SA) below 10°, endowing the surface with the so-called self-cleaning properties.[3] Researchers have revealed that the superhydrophobicity, achieved by controlling the surface compositions and the roughness structures,[4] has many potential applications in the areas of self-cleaning,[5] anti-icing,[6] anti-corrosion,[7] waterproof,[8] drag reduction[9] and water/oil separation.[10] Until now, numerous of methods are reported to fabricate superhydrophobic surfaces, including etching method,[11] spray-coating and dip-coating methods,[12] template imitated method,[13] electrospinning,[14] phase separation[15] and sol–gel process.[16] Among them, spraying-coating and dip-coating methods for the fabrication of superhydrophobic surface based on the polymer/inorganic particles seem to be the promising candidates for the widespread industrial applications due to the convenience, high efficiency, low-cost and universal applicability.[17,18]

However, the practical applications of superhydrophobic surfaces are severely limited by their poor mechanical durability, especially the scarce scratch resistance against mechanical abrasion.[19,20] The multi-level roughness structures, necessary for superhydrophobicity, are easy to be destroyed or removed even though subjected to a mild abrasion, which has a great adverse effect on the surface hydrophobicity.[21] To solve the problem, Zhu *et al.*[22] fabricated a superhydrophobic fabric with excellent mechanical stability by a facile solution-immersion process. The resultant superhydrophobic fabric could keep superhydrophobic after finger touching and abrasion against sandpaper. Meanwhile, the damaged superhydrophobic fabric could be recovered by a simple regeneration process. Li *et al.*[23] found that the superhydrophobic sponge, coated by a fluorinated-polyacrylate (PFA) and hydrophobic SiO_2 particles composite coating, showed good resistance toward sandpaper abrasion due to the inherent porous structures and

[a]College of Materials Science and Engineering, South China University of Technology, No 381, Wushan Road, Tianhe District, Guangzhou 510640, People's Republic of China. E-mail: psxrzeng@gmail.com; Fax: +86-20-87114248; Tel: +86-20-87114248
[b]National-certified Enterprise Technology Center, Kingfa Science and Technology Co., Ltd., No.33 Kefeng Road, Science Town, Guangzhou 510663, People's Republic of China

† Electronic supplementary information (ESI) available. See DOI: 10.1039/c7ra07865j

the high adhesion of PFA/SiO_2 composite to the sponge skeleton. The as-prepared sponge also possessed excellent resistance to corrosive aqueous solutions of acid, base and salt. Zhang *et al.*[24] fabricated a robust polyethersulfone (PES)/montmorillonite–silica superhydrophobic composite coating on the Al surface by combining the sol–gel and the spray-coating technology. They indicated that the enhanced abrasion resistance of the composite coating was ascribed to the lubrication performance of PES and the stable interface bonding force between the montmorillonite and SiO_2.

Although various strategies are presented to improve the mechanical durability of the surface roughness, most of the prepared superhydrophobic surfaces cannot meet the practical applications except those fabricated on the substrates that have original textured structures like fabric, meshes and porous material.[25,26] Moreover, some technologies for fabricating anti-abrasion superhydrophobic surface are only applicable to special substrates such as Al and Cu.[27,28] Thus, the facile fabrication of excellent abrasion resistance superhydrophobic coating on flat substrate still remains a great challenge. Bayer prepared the superhydrophobic coating on aluminum surface by spraying the perfluoroalkyl methacrylic copolymer (PMC) and silica (SiO_2) nanoparticles. They showed that the thermal treatment (melting) of the thermoplastic polymer was necessary to ensure the imbedding of the nanoparticle film into the polymer matrix during spraying. The resultant coating possessed good wear abrasion and substrate adhesion resistance against pencil hardness, dry/wet scribed tape peel adhesion and 17.5 kPa linear abrader tests.[29] The thermal treatment of the perfluorinated acrylic coating could also increase the resistance of the superhydrophobic surface towards fast impacting water streams.[30] In general, the abrasion resistance of the superhydrophobic surface is mainly affected by the stability of the surface structure and the adhesion strength of polymer to the substrate.[31] Most of the researchers discussed above are focused on the improvement of the bonding strength of the nanoparticles and the polymer, and the adhesion between the superhydrophobic coating and the substrate by means of the chemical bonding,[32,33] less attentions are paid to the flexibility of the polymer chains, which can reduce the surface roughness damage when suffered to abrasion because of the polymer chain deformation. Meanwhile, the fabrication methods of superhydrophobic coating with good abrasion resistance need to be simplified.

In this study, the fluorine-containing acrylates (FACs) with different T_g were synthesized by free radical initiated solution copolymerization of acrylate and fluorinated-containing monomers, and then the superhydrophobic coatings were facilely fabricated on the flat iron plate surface based on the FAC and SiO_2 particles through a two-steps spraying method. The obtained FACs were characterized by Fourier transform infrared spectroscopy (FTIR), proton nuclear magnetic resonance (^{1}H-NMR) and differential scanning calorimetry (DSC), and the superhydrophobic coatings were studied by water contact angle (WCA), scanning electron microscope (SEM) and 3D image measurement. Effects of micro-SiO_2 (M-SiO_2) content on the wetting behavior and surface morphology of the composite coating were investigated. The resistance and the mechanism of superhydrophobic coating against abrasion were also studied.

2. Experimental

2.1 Materials

Methyl methacrylate (MMA, A. R.) and butyl acrylate (BA, A. R.) were provided by Tianjin Fuchen Chemical Reagent Factory (China). Dodecafluoroheptyl methacrylate (DFMA, 96%) was got from Harbin Xeogia Fluorine–Silicon Chemical Company (China). Azodiisobutyronitrile (AIBN, A. R.) and glycidyl methacrylate (GMA, A. R.) were gained from Aladdin reagent (Shanghai) company, Limited (China). Toluene was acquired from Guangzhou chemical reagent factory (China). Hydrophobic micro-SiO_2 (OK412, diameter of about 3 μm) was purchased from Evonik degussa (Shanghai) company (China). Hydrophobic nano-SiO_2 (H17, diameter of 16–20 nm) was obtained from Wacker Chemie company (Germany).

2.2 Synthesis of FAC polymer

The fluorine-containing acrylates (FACs) with different T_g were synthesized by solution polymerization in a 500 mL four-necked glass flask equipped with a Teflon mechanical stirrer, a reflux condenser and a constant pressure funnel. Firstly, 200 g MMA and BA (with the mass ratio of 9/1, 3/2, 2/3 and 1/4), 20 g DFMA, 3 g AIBN and 250 g toluene were mechanically stirred for 15 min. Secondly, the mixture was transferred to the glass flask under mechanical agitation, and the polymerization was allowed to react at 75 °C for 3 h. Finally, the temperature of the system increased to 80 °C and the reaction was continued for another 3 h, and the FAC solution was obtained after cooling to room temperature. The synthesized FACs with different MMA/BA mass ratio of 9/1, 3/2, 2/3 and 1/4 were marked as FAC-1, FAC-2, FAC-3 and FAC-4, respectively.

2.3 Fabrication of hydrophobic coating

Firstly, the iron plates were immersed into ethanol–water solution under ultrasonic for 5 min, and washed with distilled water for three times, and dried in a clean oven at 80 °C. Subsequently, 50 g FAC solution, 50 g toluene and a certain amount of M-SiO_2 were mixed with the help of ultrasonic until the homogeneous dispersion solution was formed. Then, the mixture was sprayed on the surface of the iron plat by a spray gun, and dried at room temperature for 15 min to form the FAC/M-SiO_2 coating. Finally, the N-SiO_2 toluene dispersion with a concentration of 5 wt% N-SiO_2 was sprayed onto the FAC/M-SiO_2 coating, and the FAC/M-SiO_2/N-SiO_2 composite coating was obtained after drying at 120 °C for 2 h. It was worthy to note that the drying of the FAC/M-SiO_2 coating was necessary, otherwise most of the N-SiO_2 nanoparticles were easy to access into the FAC/M-SiO_2 coating, which had a negative effect on the formation of the nanostructures on the surface.

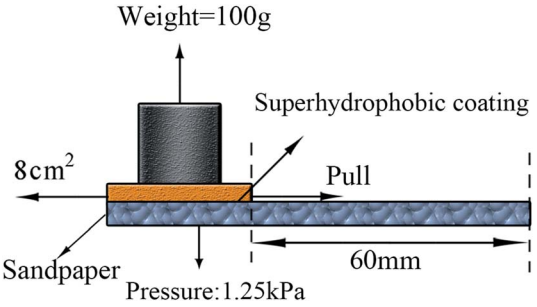

Fig. 1 Schematic of abrasion testing for superhydrophobic coating under a pressure of 1.25 kPa.

2.4 Abrasion testing

The abrasion testing was carried out according to Fig. 1, wherein the sandpaper (1200 mesh) was served as the abrasion surface. The sample was moved in one direction for 60 mm at a speed of 15 mm s^{-1} under a pressure of 1.25 kPa. Then the WCA and the surface morphology after abrasion testing were investigated.

2.5 Characterization

Fourier transform infrared spectroscopy (FTIR) spectra were recorded on a Bruker Tensor 27 spectrometer (Bruker Optics, Germany) with a spectral resolution of 4 cm^{-1} in the range from 400 to 4000 cm^{-1} using KBr pellets method.

Proton nuclear magnetic resonance (^{1}H-NMR) spectra were recorded by a Bruker AV 300 spectrometer (Bruker, Germany). The $CDCl_3$ and TMS were used as solvent and internal standard substance, respectively.

The glass transition temperature (T_g) of FAC polymer was detected by the differential scanning calorimetry (DSC, Netzch DSC-200, Germany) at a scanning rate of 20 °C min^{-1} from −50 °C to 150 °C under nitrogen atmosphere.

Water contact angle (WCA) and sliding angle (SA) were measured by a contact angle goniometer (DSA100, Germany) using 5 μL and 10 μL distilled water as indicators, respectively. Each measurement was repeated three times from different places of the sample and the average value was recorded.

3D images were taken by a SMS Expert 3D Measurement System (BMT MiniProfiler, Germany).

Surface morphologies were investigated using a field-emission scanning electron microscopy (SEM, FEI Nova Nano SEM 430, Netherlands) at an acceleration voltage of 15 kV. Samples were covered by a layer of gold before testing to prevent charging.

3. Results and discussion

3.1 FTIR

Fig. 2 showed the FTIR spectrum of FAC polymer. It could be seen that there was no peaks at 1640 cm^{-1} of –C═C– characteristic absorption in the spectrum, indicating that the monomers were completely taken part in the copolymerization. The absorptions at 2997 cm^{-1}, 2955 cm^{-1} and 2879 cm^{-1} were attributed to the stretching vibrations of $-CH_2-$ ($-CH_3$) and the peak at 1456 cm^{-1} was caused by the bending vibration of $-CH_2-$. The bands located at 1737 cm^{-1} and 1147 cm^{-1} were assigned to the C═O stretching vibration and C–O stretching vibration of esters, respectively.[34] The peaks near 1274 cm^{-1} were the characteristic absorption of the C–F bond stretching vibration and the absorption at 694 cm^{-1} was assigned to the wagging vibration of $-CF_2-$ groups.[35] Moreover, the stretching vibration of $-CF_2-$ and $-CF_3$ groups made the absorptions of 1274–1147 cm^{-1} become wide and strong, which further confirmed the existence of fluorine-containing polymer chain in the FAC. Therefore, FTIR spectrum showed that the fluorine-containing monomer had been copolymerized with the acrylate monomers.

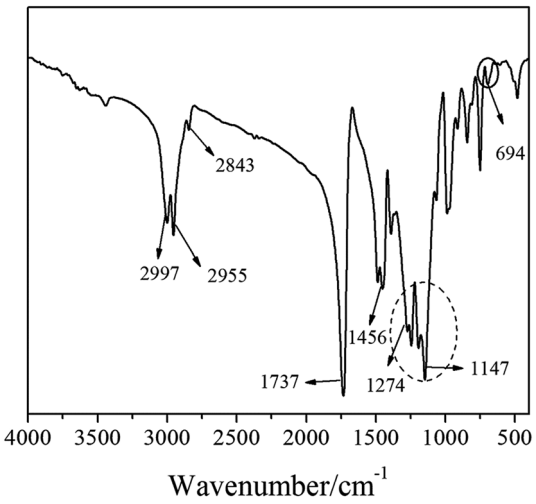

Fig. 2 FTIR spectrum of FAC polymer.

3.2 ^{1}H-NMR

The FAC structure and the corresponding peaks of ^{1}H-NMR spectrum were shown in Fig. 3. As seen from Fig. 3, the peaks

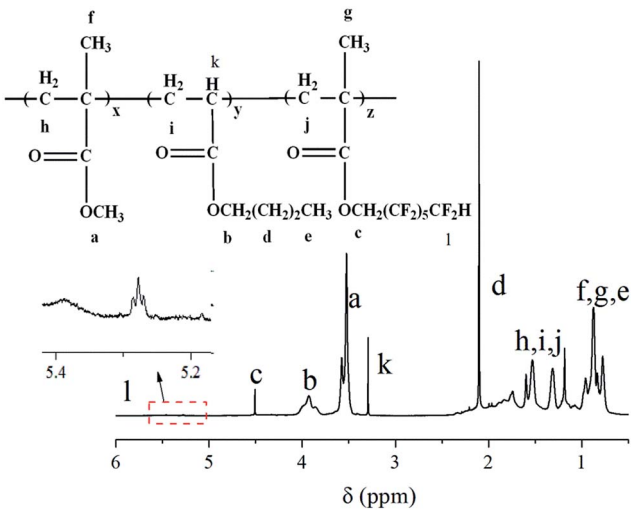

Fig. 3 ^{1}H-NMR spectrum of FAC polymer.

at $\delta = 4.5$, $\delta = 3.9$ and $\delta = 3.6$ were ascribed to the –OCH_2– from DFMA, BA and MMA, respectively. The result was in accordance with the FTIR analysis, which further confirmed that the FAC polymer was successfully synthesized.

3.3 DSC

The T_g of the FAC polymer was detected by DSC and the DSC curves were shown in Fig. 4. From Fig. 4, the theoretical T_g values of the FAC-1, FAC-2, FAC-3 and FAC-4 calculated by Fox formula were 79.3 °C, 19.8 °C, −9.8 °C and −34.0 °C, respectively. While the measured T_g values determined by DSC analysis of the FAC-1, FAC-2, FAC-3 and FAC-4 were 74.2 °C, 24.5 °C, −7.7 °C and −29.5 °C, respectively. As the T_g of the polymer was not only affected by the flexibility of polymer chain, but also affected by the polymer molecular weight and its distribution, there was a little difference between theoretical value and measured value. It showed that the measured values were accordance with the theoretical values, indicating that the targeted FAC polymers were obtained.

3.4 Water contact angle

Fig. 5 showed the effects of M-SiO_2 content on the WCA of FAC-4/M-SiO_2 and FAC-4/M-SiO_2/N-SiO_2 composite coatings. As shown in Fig. 5, the surface of the FAC-4 coating was hydrophobic with a WCA of about 97°, owing to the good repellent property of fluorine chains in the FAC-4. With the increase of M-SiO_2 content from 3 wt% to 12 wt%, the WCA on the surface gradually enlarged from 103° to 115°. Although the addition of M-SiO_2 particles on the surface was good for the construction of roughness and the increase of WCA, the surface was hard to achieve superhydrophobic because the micro structure roughness was insufficient.[36] Inspired from the lotus leaves and butterfly wings, the micro–nano or hierarchical structures were the keys for the superhydrophobicity.[37] It was shown that the special micro–nano structures could be generated by the spraying of N-SiO_2 particles on the surface.[17] In Fig. 5, after spraying with N-SiO_2 particles, for the FAC-4/N-SiO_2 coating, its WCA increased to 152.3°, and all of the FAC-4/M-SiO_2/N-SiO_2 composite coatings became superhydrophobic with a WCA higher than 150°, which indicated the formation of hierarchical micro–nano structures on the surface.

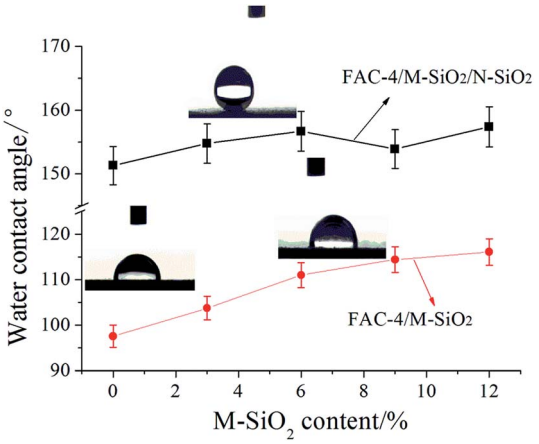

Fig. 5 Effects of M-SiO_2 content on the WCA of FAC-4/M-SiO_2 and FAC-4/M-SiO_2/N-SiO_2 composite coating.

3.5 Water adhesive force and sliding angle

Photos of water droplet got in touch with superhydrophobic coating and the SA of superhydrophobic surface (f) were shown in Fig. 6. In Fig. 6 (a–e), when a water droplet was extruded from the needle tubing, it would keep spherical and stuck on the needle tubing due to the high surface tension of water. The superhydrophobic coating was forced to get in touch with the water droplet, and the water droplet could not spread over or wet the surface. In addition, in Fig. 6(f), the water droplet was easy to slide away from the surface when it inclined at a little angle less than 5°, owing to the special water repellent property on the surface. It showed that the superhydrophobic coating possessed low water adhesive force and SA.

3.6 SEM

Fig. 7 showed the SEM images of FAC, FAC-4/M-SiO_2 and FAC-4/M-SiO_2/N-SiO_2 coatings. As shown in Fig. 7(a), the surface of the FAC-4 coating was rather smooth and no obvious bulges could be seen. When 6 wt% M-SiO_2 particles was added, in Fig. 7(b), there were many bumps of M-SiO_2 particles in micro sizes of about 3–5 μm appeared on the surface, resulting in the increase of surface roughness and WCA. However, the introduction of M-SiO_2 could not meet the requirement of superhydrophobicity because of the inadequate roughness on the surface. After coating with N-SiO_2 particles, as shown in Fig. 7(c), a plenty of mountain like protrusions in micro sizes were attached on the surface and the high resolution inserted in Fig. 7(c) confirmed that the protrusions were mainly composed of N-SiO_2 particles in nano size, indicating that the N-SiO_2 particles got together as micro aggregates to form micro–nano structures on the surface. Thus, the binary micro/nano structure and the low surface energy made contributions to the superhydrophobicity of the FAC-4/N-SiO_2

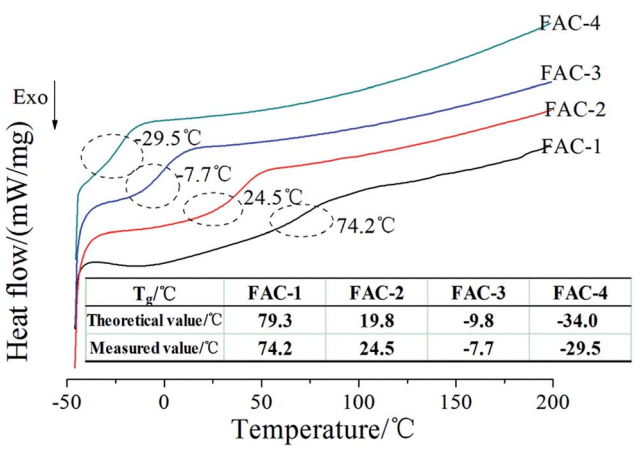

T_g/℃	FAC-1	FAC-2	FAC-3	FAC-4
Theoretical value/℃	79.3	19.8	-9.8	-34.0
Measured value/℃	74.2	24.5	-7.7	-29.5

Fig. 4 DSC curves of the FAC polymers.

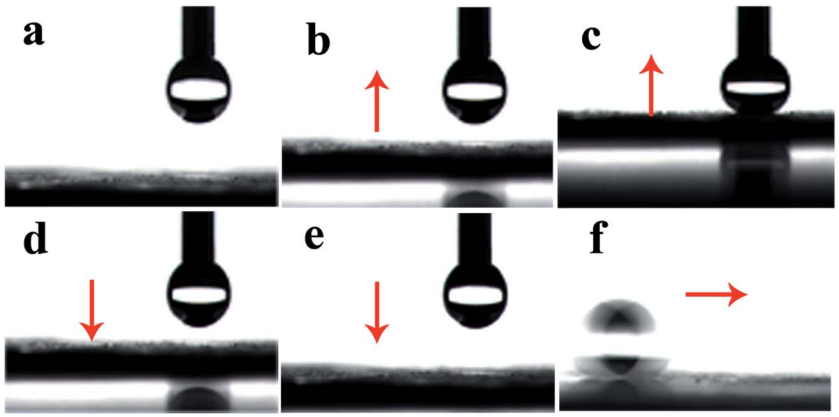

Fig. 6 Process of water droplet got in touch with superhydrophobic FAC-4/M-SiO_2/N-SiO_2 coating (a–e) and the SA on the superhydrophobic surface (f).

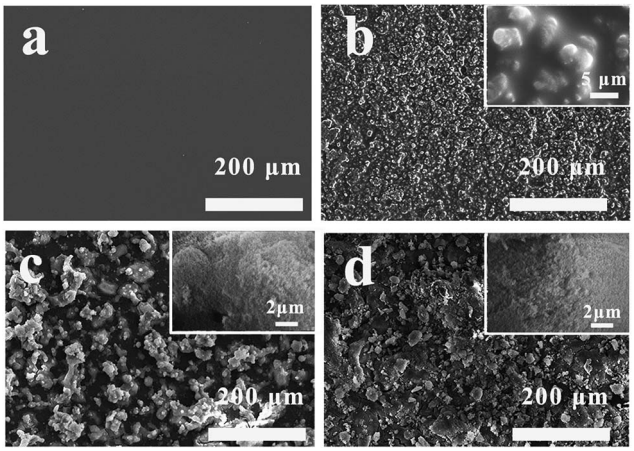

Fig. 7 SEM images of FAC, FAC-4/M-SiO_2 and FAC-4/M-SiO_2/N-SiO_2 coatings. (a) FAC-4; (b) FAC-4/M-SiO_2 coating (the M-SiO_2 content was 6 wt%); (c) FAC-4/N-SiO_2 coating; (d) FAC-4/M-SiO_2/N-SiO_2 (the M-SiO_2 content was 6 wt%).

coating.[17] In Fig. 7(d), as the surface of FAC/M-SiO_2 was coated with N-SiO_2 particles, the surface exhibited similar morphology in comparison with the Fig. 7(c), and showed superhydrophobic with a WCA of 153.1°.

3.7 3D measurement

Fig. 8 showed the 3D images of the FAC-4 film (a) and FAC-4/M-SiO_2/N-SiO_2 composite coating (b). In Fig. 8(a), the surface of FAC-4 was relative flat with a surface roughness (S_a) of 0.38 mm. However, for the FAC-4/M-SiO_2/N-SiO_2 composite coating, some of the mountains like protrusions and bumps could be seen and the surface became rather rough with a S_a of about 1.23 mm, which provided sufficient roughness for superhydrophobicity. The 3D measurement results further confirmed the formation of binary hierarchical structures on the superhydrophobic surface.

3.8 Wetting behavior after abrasion testing

As shown in Fig. 9, all of the superhydrophobicity of composite coatings were destroyed after abrasion. With the decrease of T_g of FAC from 74.2 °C to −29.5 °C, the WCA of the FAC/N-SiO_2 coatings increased from 117.2° to 128.4° while the FAC/M-SiO_2/N-SiO_2 enlarged from 127.3° to 144.1°. Moreover, for the FAC/N-SiO_2 coatings, the water droplets were sticky on the surface even though the surfaces were turned up side down, while for the FAC-3/M-SiO_2/N-SiO_2 and FAC-4/M-SiO_2/N-SiO_2, the SAs were 80° and 38°, respectively. In general, water droplets were always sticky on the superhydrophobic surface even if the WCA

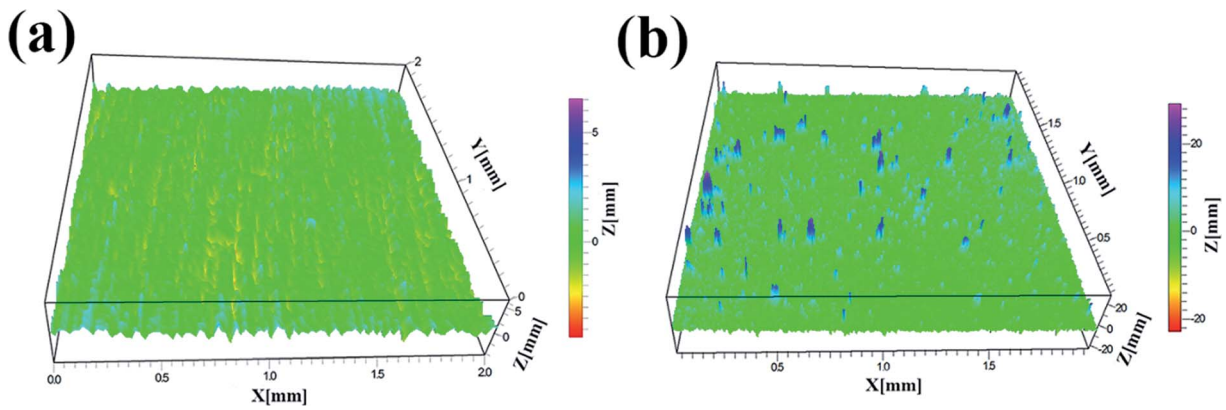

Fig. 8 3D images of FAC-4 film (a) and FAC-4/M-SiO_2/N-SiO_2 coating (b).

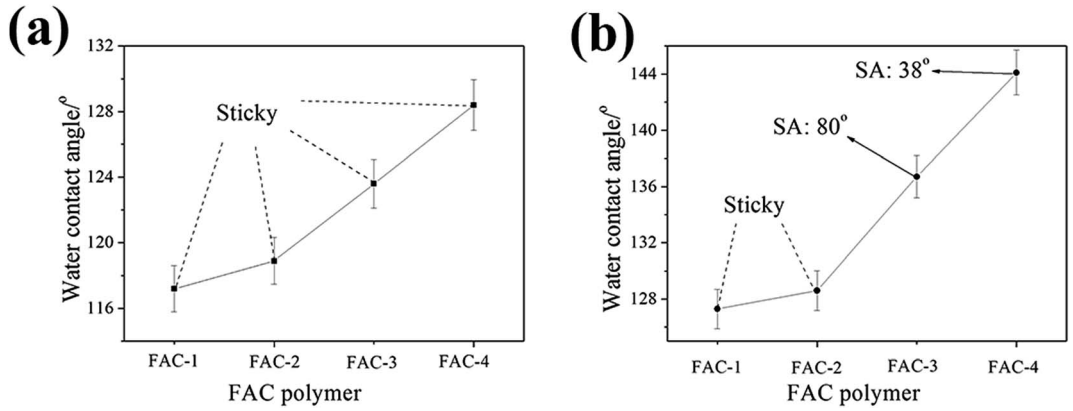

Fig. 9 Wetting behavior of FAC/N-SiO_2 (a) and FAC/M-SiO_2/N-SiO_2 (b) after abrasion.

had a slight decrease after the abrasion. The SA was more sensitive to the change of the surface micro/nano structures than the WCA, which implied that the superhydrophobic surface had a low SA after abrasion testing possessed good abrasion resistance.[38] Hence, the superhydrophobic coating fabricated based on the FAC polymer with lower T_g had better anti-abrasion property. Meanwhile, it was obvious that the FAC/M-SiO_2/N-SiO_2 had higher WCA than that of the FAC/N-SiO_2 when using the same FAC polymer, which indicated that the existence of M-SiO_2 particles in the composite could reduce the negative impacts on the WCA after abrasion.

3.9 Surface morphology and WCA after abrasion testing

As shown in Fig. 10(a), after 1 cycles of abrasion testing, only little N-SiO_2 particles could be observed on the surface of FAC-1/N-SiO_2 coating, and most of the N-SiO_2 particles was severely abraded, leading to the dramatic decrease of WCA to 117.2°. While in Fig. 8(b) of FAC-4/N-SiO_2 surface, it showed that the scattered micro-nano N-SiO_2 aggregates were connected with each other, and the bigger aggregates were formed on the surface. Meanwhile, the roughness of the surface was smoothed after the abrasion testing, which made the WCA of the surface decrease to 128.4°. It could be derived that the surface of FAC-4 with low T_g was sticky at room temperature, which could prevent the N-SiO_2 particles from detaching from the surface. In Fig. 10(c), for FAC/M-SiO_2/N-SiO_2 coating, although part of the surface roughness was smoothed, it could be seen that some of the protrusions was attached onto the surface. As shown in Fig. 10(d) in high resolution, there were many N-SiO_2 particles tightly adhered to the M-SiO_2 particles because of the adhesion of FAC-4 polymer. Compared with the FAC-4/N-SiO_2 coating, the M-SiO_2 particles provided micro-structure on the surface and could weaken the abrasion force to the surface micro roughness damage. These micro–nano structures made the surface show good hydrophobicity with a high WCA of 144.1°, only a slight decrease in comparison with the untested surface. It had been proven that the micro–nano structures were essential to keep the high WCA of the surface after abrasion testing.[39] The results showed that the superhydrophobic FAC-4/M-SiO_2/N-SiO_2 coating had good abrasion resistance, which allowed the coatings to be used in practical applications.

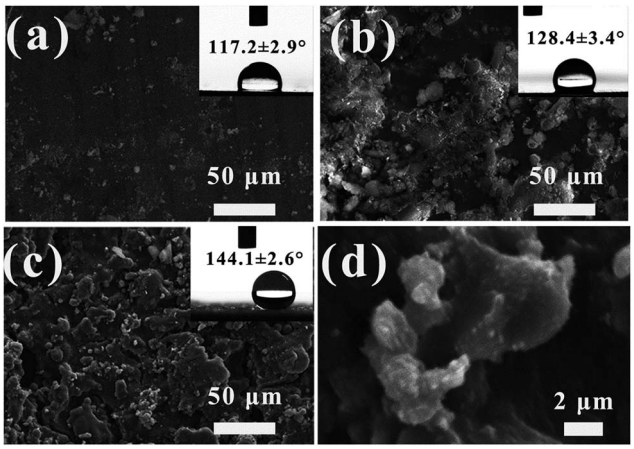

Fig. 10 SEM images and WCAs of FAC/N-SiO_2 and FAC M-SiO_2/N-SiO_2 composite coatings after abrasion testing. (a) FAC-1/N-SiO_2; (b) FAC-4/N-SiO_2; (c and d) FAC-4/M-SiO_2/N-SiO_2 (the M-SiO_2 content was 6 wt%).

3.10 Mechanism of superhydrophobic coating against abrasion

The mechanism of superhydrophobic coating against abrasion was presented in Fig. 11. As shown in Fig. 11(a), for FAC-1/N-SiO_2 coating with high a T_g of 74.2 °C, the N-SiO_2 particles were difficult to permeate into the surface due to the poor motion ability of polymer chains at room temperature, and they were mainly attached on the surface of FAC-1 with poor adhesion. After abrading by the sandpaper, the N-SiO_2 particles were abraded away from the surface, resulting in the dramatic decrease of WCA. In Fig. 11(b), for FAC-4 coating with low a T_g of −29.5 °C, the polymer chains were easy to move to offer potential penetration of N-SiO_2 particles into the surface and part of N-SiO_2 particles and aggregates sank into the surface of FAC-4 coating, which was beneficial for the increase of adhesive force between N-SiO_2 particles and polymer chains. Meanwhile, the surface tackiness could prevent the detachment of N-SiO_2

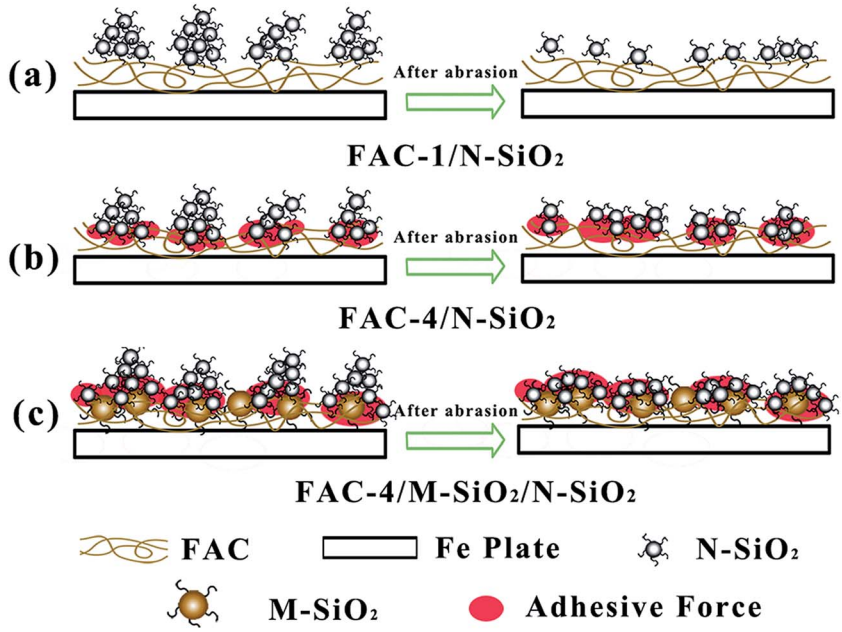

Fig. 11 Mechanism of superhydrophobic coating against abrasion.

particles from the surface during abrasion, and kept the surface roughness required for good hydrophobicity. Although the N-SiO_2 particles were attached on the FAC-4 surface after abrasion, the N-SiO_2 aggregates with micro sizes were easy to be smoothed, which would destroy the binary micro/nano roughness and the WCA of the surface. In Fig. 11(c), for FAC-4/M-SiO_2/N-SiO_2 coating, the existence of M-SiO_2 particles could provide the micro-structure and weaken the abrasion force to the surface roughness damage during abrasion, which ensured the binary micro/nano structures and kept the high hydrophobicity of the surface.

4. Conclusions

The FACs with different T_g were successfully synthesized by solution copolymerization, and then the superhydrophobic coatings were fabricated based on the FACs and SiO_2 particles through a two-steps spraying method. FTIR and ^{1}H-NMR showed that the fluorinated-containing monomer was copolymerized with the acrylate monomers, and the FACs with different T_g of about 74.2 °C, 24.5 °C, −7.7 °C and −29.5 °C were prepared. With the increase of M-SiO_2 content from 3 wt% to 12 wt%, the WCA on the surface gradually enlarged from 103° to 115°, indicating that the micro structures were insufficient for superhydrophobicity. After coating with N-SiO_2 particles, all the surfaces of FAC-4 and FAC-4/M-SiO_2 showed binary nano/microstructures and became superhydrophobic with a WCA higher than 150°. The obtained superhydrophobic coating also possessed low water adhesive force and SA. Abrasion testing showed that the superhydrophobic coating fabricated based on the FAC polymer with low T_g had good abrasion resistance, and the incorporation of M-SiO_2 particles could weaken the abrasion force to the surface roughness damage and acted as connections for the adhesion of N-SiO_2 particles during abrasion, which ensured the micro–nano structures on the surface after abrasion testing. The obtained abrasion resistance superhydrophobic coating could be fabricated on various flat substrates through a facile spray method and had great potential applications.

Conflicts of interest

There are no conflicts to declare.

Acknowledgements

Thanks for the device supports from National-certified Enterprise Technology Center, Kingfa Science and Technology Co., Ltd., and the financial supports by the National Natural Science Foundation of China (51403067, 51573052) and the Pearl River S&T Nova Program of Guangzhou (201710010062).

References

1 S. Nishimoto and B. Bhushan, *RSC Adv.*, 2013, **3**, 671–690.
2 E. J. Falde, S. T. Yohe, Y. L. Colson and M. W. Grinstaff, *Biomaterials*, 2016, **104**, 87–103.
3 T. L. Sun, G. Y. Qing, B. L. Su and L. Jiang, *Chem. Soc. Rev.*, 2011, **40**, 2909–2921.
4 Y. B. Zhang, Y. Chen, L. Shi, J. Li and Z. G. Guo, *J. Mater. Chem.*, 2012, **22**, 799–815.
5 I. P. Parkin and R. G. Palgrave, *J. Mater. Chem.*, 2005, **15**, 1689–1695.
6 K. Q. Li, X. R. Zeng, H. Q. Li and X. J. Lai, *Appl. Surf. Sci.*, 2015, **346**, 458–463.
7 S. Yu and Z. G. Guo, *RSC Adv.*, 2015, **5**, 107880–107888.

8 Y. Li, B. Ge, X. H. Men, Z. Z. Zhang and Q. J. Xue, *Compos. Sci. Technol.*, 2016, **125**, 55–61.
9 H. Park, G. Y. Sun and C. J. Kim, *J. Fluid Mech.*, 2014, **747**, 722–734.
10 K. Q. Li, X. R. Zeng, H. Q. Li, X. J. Lai and H. Xie, *Mater. Lett.*, 2014, **120**, 255–258.
11 Y. H. Xiu, L. B. Zhu, D. W. Hess and C. P. Wong, *Nano Lett.*, 2007, **7**, 3388–3393.
12 Z. L. Chu and S. Seeger, *RSC Adv.*, 2015, **5**, 21999–22004.
13 Y. Li, Z. Z. Zhang, B. Ge, X. H. Men and Q. J. Xue, *Green Chem.*, 2016, **18**, 5266–5272.
14 L. Jiang, Y. Zhao and J. Zhai, *Angew. Chem., Int. Ed.*, 2004, **116**, 4438–4441.
15 S. T. Aruna, P. Binsy, E. Richard and B. J. Basu, *Appl. Surf. Sci.*, 2012, **258**, 3202–3207.
16 H. Budunoglu, A. Yildirim, M. O. Guler and M. Bayindir, *ACS Appl. Mater. Interfaces*, 2011, **3**, 539–545.
17 K. Q. Li, X. R. Zeng, H. Q. Li and X. J. Lai, *Appl. Surf. Sci.*, 2014, **298**, 214–220.
18 Y. Li, X. H. Men, X. T. Zhu, B. Ge, F. J. Chu and Z. Z. Zhang, *J. Mater. Sci.*, 2016, **51**, 2411–2419.
19 A. Milionis, E. Loth and I. S. Bayer, *Adv. Colloid Interface Sci.*, 2016, **229**, 57–79.
20 J. H. Zhi, L. Z. Zhang, Y. Y. Yan and J. Zhu, *Appl. Surf. Sci.*, 2017, **392**, 286–296.
21 X. L. Tian, T. Verho and R. H. A. Ras, *Science*, 2016, **352**, 142–143.
22 X. T. Zhu, Z. Z. Zhang, J. Yang, X. H. Xu, X. H. Men and X. Y. Zhou, *J. Colloid Interface Sci.*, 2012, **380**, 182–186.
23 K. Q. Li, X. R. Zeng, H. Q. Li and X. J. Lai, *RSC Adv.*, 2014, **4**, 23861–23868.
24 X. G. Zhang, H. Y. Wang, Z. J. Liu, Y. X. Zhu, S. Q. Wu, C. J. Wang and Y. J. Zhu, *Appl. Surf. Sci.*, 2017, **396**, 1580–1588.
25 A. M. Rather and U. Manna, *Chem. Mater.*, 2016, **28**, 8689–8699.
26 L. X. Li, B. C. Li, L. Wu, X. Zhao and J. P. Zhang, *Chem. Commun.*, 2014, **50**, 7831–7833.
27 B. B. Zhang, X. Zhao, Y. T. Li and B. R. Hou, *RSC Adv.*, 2016, **6**, 35455–35465.
28 J. H. Zhi, L. Z. Zhang, Y. Y. Yan and J. Zhu, *Appl. Surf. Sci.*, 2017, **392**, 286–296.
29 I. S. Bayer, K. G. Krishnan, R. Robison, E. Loth, D. H. Berry, T. E. Farrell and J. D. Crouch, *Sci. Rep.*, 2016, **6**, 38459.
30 I. S. Bayer, A. J. Davis and A. Biswas, *RSC Adv.*, 2014, **4**, 264–268.
31 A. Milionis, J. Languasco, E. Loth and I. S. Bayer, *Chem. Eng. J.*, 2015, **281**, 730–738.
32 Z. Wang, H. B. Zhu, N. Cao, R. K. Du, Y. Q. Liu and G. Z. Zhao, *Mater. Lett.*, 2017, **186**, 274–278.
33 I. S. Bayer, *Coatings*, 2017, **7**, 12.
34 X. Y. Xiao and Y. Wang, *Colloids Surf., A*, 2009, **348**, 151–156.
35 W. Xu, Q. F. An, L. F. Hao, D. Zhang and M. Zhang, *Appl. Surf. Sci.*, 2013, **268**, 373–380.
36 K. Q. Li, X. R. Zeng, H. Q. Li, X. J. Lai, C. X. Ye and H. Xie, *Appl. Surf. Sci.*, 2013, **279**, 458–463.
37 K. Koch, B. Bhushan, Y. C. Jung and W. Barthlott, *Soft Matter*, 2009, **5**, 1386–1393.
38 H. Y. Wang, Y. X. Zhu, Z. Y. Hu, X. G. Zhang, S. Q. Wu, R. Wang and Y. J. Zhu, *Chem. Eng. J.*, 2016, **303**, 37–47.
39 J. H. Zhi, L. Z. Zhang, Y. Y. Yan and J. Zhu, *Appl. Surf. Sci.*, 2017, **392**, 286–296.